A Computational Model of Osteochondral Defect Repair Using a Tissue Engineered Scaffold.

Abstract

Tissue engineering (TE) has recently emerged as a potential method with which to treat osteochondral defects. In order to improve these strategies, an understanding is required of how the cells within an implanted scaffold interact with their local environment. To this end, the objective of this study was to develop a computational model of an osteochondral defect following the implantation of a tissue engineered scaffold. In particular, the purpose of this was to systematically explore the relationship that scaffold design has on the spatial formation of cartilage and bone within the defect. In this study, tissue formation was predicted using a previously developed algorithm in which cell fate was dependent upon the local oxygen tension and the local mechanical environment. In the first part of this study, the model was updated to include a condition whereby mature cartilage was resistant to both terminal differentiation and vascularisation. The updated model was then tested by using it to predict tissue formation during the spontaneous repair process within an osteochondral defect. Following this, the model was used to simulate an osteochondral defect treated with different variations of a previously developed multiphasic scaffold. By comparing the results of the different simulations it was possible to elucidate a mechanism by which the scaffold promoted robust bone and cartilage formation. In particular, support was provided for a previous hypothesis which proposed that osteochondral defect repair can be enhanced by actively confining angiogenesis to within the subchondral region of the defect for a sustained period of time. Based on the results of this study, it was possible to expand on this by suggesting that this time period be no less than 10 weeks. It is possible to reduce this, however, by pre-culturing MSCs under chondrogenic conditions prior to implantation within the defect.

1 Introduction

In recent years tissue engineering (TE) has emerged as a viable strategy for the treatment of osteochondral defects (1). The goal of these strategies is to use cells, scaffolds and growth factors to regenerate the damaged tissue and thus provide long term relief to the patient (2). While numerous advances have been made in the design of multiphasic scaffolds (3–5), cell culture protocols (6,7) and growth factor releasing materials (8,9), a number of issues still exist which limit the widespread implementation of these techniques. One of the most prominent of these is promoting the formation of stable bone and cartilage within the osseous and chondral regions of the defect respectively. In particular, the cartilage that forms within the chondral region of an osteochondral defect must be resistant to terminal differentiation in order to prevent the upward migration of the bone plate (10), a phenomena which has been hypothesised to contribute to the eventual break down of the repair tissue (11).

In an effort to better understand the factors which promote a stable cartilage phenotype, a number of studies have explored the influence of various environmental and culture conditions on chondrogenesis and hypertrophy of adult stem cells (6,12–14). Liu *et al.* (12) demonstrated that mesenchymal stem cell (MSC) derived chondrocytes were resistant to both mineralisation and vascularisation if cultured in chondrogenic media for 12 weeks *in vitro* prior to subcutaneous implantation. As an extension of this, it was then demonstrated that MSCs maintained *in vitro* in hypoxic conditions remained cartilaginous *in vivo*, demonstrating that oxygen tension is a key regulator of the chondrogenic phenotype (15). Recognising such a relationship between vascularisation, oxygen and chondrocyte hypertrophy (16,17), a number of studies have reported improved cartilage formation in an osteochondral defect following the application of anti-angiogenic factors (18–21). Other studies have attempted to alter the physical characteristics of scaffolds to mimic the calcified layer that separates cartilage and bone in the osteochondral unit (22), thereby creating unique oxygen and nutrient environments in each region of a regenerating osteochondral defect.

While together such studies have improved the understanding of how environmental factors regulate MSC fate, it is particularly difficult to systemically explore how the design of scaffolds and engineered constructs regulates osteochondral defect regeneration. The objective of this study was thus to provide a mechanistic approach to explain how design

changes to scaffolds might either enhance or impair osteochondral defect regeneration. To this end, a previously developed computational model of osteochondral defect repair was utilised. As part of this model, cell fate was regulated by the local oxygen tension and the mechanical environment (substrate stiffness and tissue strain). In the first part of this study, motivated by the findings of Liu *et al.* (12), the model of angiogenesis was extended to include a rule whereby blood vessel growth into regions of mature cartilage was inhibited. This model was developed by using it to predict the observed course of tissue formation during the spontaneous repair process within an osteochondral defect. The utility of the model was then demonstrated by using it to simulate osteochondral defect repair following the implantation of different variations of a scaffold developed by Da *et al.* (22). The premise of this scaffold was that it incorporated a compact layer which mimicked the calcified cartilage interface between the osseous and the chondral phases. We hypothesised that, during the early stages of healing, this compact layer serves to limit angiogenesis to the osseous phase of the defect. This confinement of angiogenesis then allows seeded MSCs in the chondral phase to form stable cartilage which, following the absorption of the compact layer, are resistant to both vascularisation and mineralisation.

2 Method

2.1 Scaffold Design

Two different tissue engineered scaffold designs were developed in the study conducted by Da et al. (22). The first was a bilayer scaffold composed of an osseous and a chondral phase bonded directly to each other. The second was a trilayer scaffold composed of an osseous and a chondral phase separated by an impermeable compact layer. In both scaffolds the osseous layer was formed from a composite scaffold fabricated from PLGA/TCP skeleton wrapped in type I collagen (23) while the chondral layer was manufactured from bovine cartilage extra cellular matrix (24). The compact layer was formed from dense PLGA/TCP and was shown to be impermeable (22). Prior to implantation, bone marrow derived MSCs were seeded onto the different phases of the scaffold (5×10^5 cells on the osseous phase and 2×10^5 cells on the chondral phase) (22). Following this, a custom made bioreactor was used to culture the cells *in vitro* in either osteogenic or chondrogenic media for a period of 21 days depending on whether they were in the osseous or the chondral phase respectively.

2.2 Iterative Procedure

Tissue differentiation was simulated over a 24 week period in an empty osteochondral defect or a scaffold treated defect using an iterative procedure similar to the one outlined by Burke *et al.* (25) (Supplementary Material Section 8.1). In the developed models, each iteration simulated a time period of 24 hours. As part of this, a finite element (FE) model was used to predict the mechanical environment within the defect while an oxygen diffusion model was used to predict the local oxygen tension. The results of these simulations were used as inputs to models of angiogenesis and cell migration, proliferation, death and differentiation.

Table 1: Material Parameters

Material Property	Granulation Tissue	Fibrous Tissue	Fibro-Cartilage	Cartilage	Hypertrophic Cartilage	Immature Bone	Mature Bone	Cortical Bone
Young's Modulus [MPa]	1[a]	2[a,b]	5	10[a,b]	20	1000[a]	6000[c]	20,000[c]
Poisson's Ratio	0.167[a]	0.167[a]	0.167	0.167[a]	0.167	0.3[a]	0.3[a]	0.3[a]
Permeability [mm^4/ Ns]	0.01[a]	0.01[a,b]	0.01	0.005[a,b]	0.005	0.1[a]	0.0037	1e-5[a]
Solid Volume Fraction	0.2[a]	0.2[a]	0.2	0.2[a]	0.2	0.2[a]	0.2[a]	0.2[a]

[a] (26)
[b] (27)
[c] (28)

2.3 Finite Element Models

A simplified 3D FE model of an osteochondral defect within the femoral condyle was constructed using the FE package FEBio (version 2.2.2, University of Utah, Technology Commercialization Office, 615 Arapeen Drive, Suite 310, Salt Lake City). This model was used to predict the biophysical stimuli generated within such a defect during gait (Figure 1). The developed model had the same geometry as outlined in a previous study. All materials were modelled as bi-phasic, except for the meniscus which was modelled as a transversely isotropic elastic material with a higher stiffness in the circumferential direction ($E^x = E^z = 20$ MPa; $E^y = 140$ MPa; $v^{xy} = 0.2$; $v^{yz} = 0.49$; $G^{xy} = 50$ MPa) (29). A sliding interface was used to model the contact between the meniscus and the cartilage layer. A defect of size ϕ5 mm x 5 mm was included at the centre of the condyle. Depending on the simulation, this was assumed to be initially filled with granulation tissue (in the case of an empty defect) or either of the scaffolds

developed by Da et al. (22). The material properties of each tissue type are listed in Table 1. A load of 2400 N was applied over 1 second based on the assumption of five to six times subject weight (80 kg) spread evenly between the lateral and medial compartments [14].

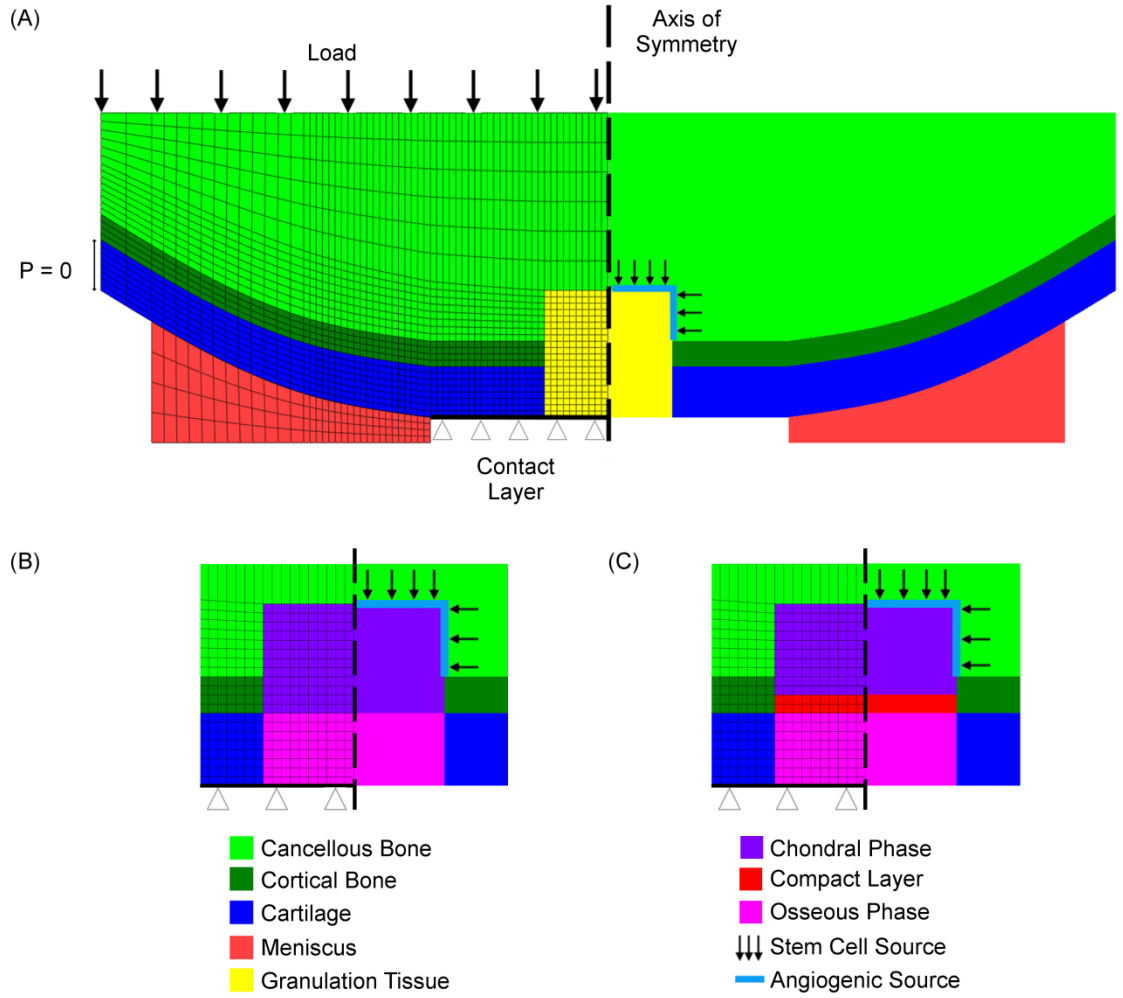

Figure 1: FE model and boundary conditions of an osteochondral defect for the simulations of (A) the spontaneous repair process and tissue formation following the implantation of the (B) bilayer scaffold and (C) trilayer scaffold , similar to that developed by Da et al. (22).

2.3.1 Finite Element Models of Scaffold Treated Defects

The scaffolds had the same dimensions as the defect and it was assumed that the repair tissue bonded directly to the native tissue (Figure 1B & C). For the bilayer scaffold model, the osseous phase was the same height as the native bone (3 mm) while the chondral phase was the same height as the native cartilage (2 mm). In the trilayer scaffold model the osseous phase had a height of 2.5 mm, the compact layer had a thickness of 0.5 mm and the chondral phase had a height of 2 mm. All of the scaffold materials were modelled as bi-phasic where the solid phase was assumed to be isotropic elastic. At day 0, the material parameters for the osseous phase were E = 20 MPa, k = 1 $mm^4 N^{-1} s^{-1}$, ν = 0.167 and ϕ = 0.9 (23). The compact

layer had the same properties except k = 0.00001 $mm^4\ N^{-1}\ s^{-1}$ and ϕ = 0.99. Finally, for the chondral layer E = 2 MPa, k = 1 $mm^4\ N^{-1}\ s^{-1}$, ν = 0.167 and ϕ = 0.9 (24). The scaffold material parameters were updated iteratively in the same way as for the spontaneous repair model. Regarding the trilayer scaffold group, the material parameters of the compact layer remained constant for a period of time ($T^{degrade}$). After this point the material in the compact layer was assumed to start resorbing and cells were able to migrate into the vacant space. The material parameters in these elements were then updated accordingly.

2.4 Angiogenesis

Angiogenesis was modelled using the lattice based approach described by Checa *et al.* (30). Furthermore the rules governing blood vessel growth and direction were the same as those outlined in our previous study (31). Similar to the method described by Carlier *et al.* (32), it was assumed that blood and nutrients could only flow through vessels which had formed a closed loop. Based on this, the ECs which made up a blood vessel were considered inactive until anastomosis had occurred.

As part of this study an additional feature was added to the model whereby blood vessel growth was inhibited by stable cartilage (33–36). It was thus assumed that blood vessels stopped growing if they entered an element which had been classified as cartilage for a sustained period of time (T^{stable}).

2.5 Cell Migration, Cell Proliferation and Cell Death

The migration and proliferation of MSCs, osteoblasts (OBs), chondrocytes (CCs), fibroblasts (FBs), hypertrophic chondrocytes (HC) and fibrochondrocytes (FCs) was also modelled using a lattice approach (30,37). The migration of cells was implemented using 'random walk' theory (37). Cell proliferation was implemented in a similar fashion provided that there was a vacant position beside the parent cell. Cell proliferation was inhibited in regions where the oxygen concentration fell below a specific threshold value (O_2^{prolif}) (**Error! Reference source not found.**). The maximum number of cells allowed in any element was limited to 1×10^5 cells/mm^3 (25). The migration rate (M) determined the number of attempted migration actions per time step while the doubling time (DT) was the age a cell had to be before it proliferated (**Error! Reference source not found.**). If the oxygen concentration fell below a threshold value (O_2^{death}) then cell death was initiated.

Table 2: Angiogenesis and MSC Differentiation Model Parameters

Model Parameter	Symbol	Source	Unit	Value
Octahedral shear strain threshold for inhibition of angiogenesis	ε^{angio}	Estimated	-	0.1
Blood vessel growth rate	V^{growth}	Estimated	mm day^{-1}	0.1
Minimum length for branching	L_{min}	(30)	mm	0.2
Maximum length without branching	L_{max}	(30)	mm	0.5
Oxygen diffusion coefficient	G	(25,38)	mm^2 s^{-1}	2.2E-03
Initial oxygen tension	$O_2^{initial}$	(39)	mol mm^{-3}	101.6E-12
Oxygen tension for inhibition of differentiation	$O_2^{inhibition}$	(40)	mol mm^{-3}	5.48E-12
Oxygen limit for cartilage	$O_2^{cartilage}$	(25)	mol mm^{-3}	30E-12
Oxygen limit for differentiation of immature cartilage to hypertrophic cartilage	$O_2^{hypertrophic}$	Estimated	mol mm^{-3}	30E-12
Strain threshold above which chondrocyte hypertrophy was inhibited	$\varepsilon^{hypertrophic}$	Estimated	%	5
Strain threshold above which fibrocartilage formed	$\varepsilon^{fibrocartilage}$	Estimated	%	12.5
Oxygen limit for differentiation of stable cartilage to hypertrophic cartilage	$O_2^{hyp,\ stable}$	Estimated	mol mm^{-3}	50.48E-12
Time required for stable cartilage to form	T^{stable}	(6,12–14)	weeks	8 - 12
Oxygen limit for calcification of hypertrophic cartilage	$O_2^{endochondral}$	Estimated	mol mm^{-3}	50.48E-12
Time before the compact layer starts to degrade	$T^{degrade}$	Estimated	weeks	0 - 8

2.6 Oxygen Transport

Oxygen transport was modelled using the same method outlined in a previous study (31). Briefly, the cellular consumption of oxygen was modelled separately for each cell phenotype using Michealas-Menten kinetics (Table 4) while the oxygen supply from the vascular network was determined using a production term which was updated based on the number of active ECs within an element (Supplementary Material: Section 8.2).

Table 3: Cell Model Parameters

Model Parameter	MSC	CC	OB	FB	HC	FC
Doubling Time [days]	0.5[a]	1.5[a]	1[a]	0.5[a]	1.5[a]	1.5
Migration Rate [μm/hr]	26.6[b]	N/A	N/A	26.6[b]	N/A	N/A
O_2 Concentration for Cell Proliferation [mol mm^{-3}]	40 $x10^{-12}$ [c]	10 $x10^{-12}$	80 $x10^{-12}$ [c]	20 $x10^{-12}$	30 $x10^{-12}$	10 $x10^{-12}$
O_2 Concentration for Cell Death [mol mm^{-3}]	5 $x10^{-12}$	5 $x10^{-12}$	20 $x10^{-12}$ [d]	5 $x10^{-12}$	5 $x10^{-12}$	5 $x10^{-12}$
Anoxic Death Rate [% cells day^{-1}]	20	20	20	20	20	20

[a] (41)
[b] (42)
[c] (43)
[d] (44)

Table 4: Oxygen parameters for each cell phenotype

Michealas - Menten Parameters	MSC	CC	OB	FB	HC	FC
Cell type (n)	1	2	3	4	5	6
Max O_2 Consumption Rate (Q_{max}) [mol $cell^{-1}$ hr^{-1}]	93.2 $x10^{-15}$ [a]	1.8 $x10^{-15}$ [a, b]	93.2 $x10^{-15}$ [a]	93.2 $x10^{-15}$ [a]	1.8 $x10^{-15}$ [a]	1.8 $x10^{-15}$ [a, b]
O_2 Concentration at half max consumption (K^m) [mol mm^{-3}]	22.5 $x10^{-12}$	22.5 $x10^{-12}$	22.5 $x10^{-12}$	22.5 $x10^{-12}$	22.5 $x10^{-12}$	22.5 $x10^{-12}$

[a] (32)
[b] (43)

2.7 MSC Differentiation and Chondrocyte Hypertrophy

MSC differentiation was determined using an updated version of the tissue differentiation algorithm developed by Burke *et al.* (25). Briefly, MSC fate was governed by the substrate stiffness and the local oxygen tension (Supplementary Material: Section 8.3) while the chondrogenic phenotype was affected by the magnitude of the local octahedral shear strain and the local oxygen tension (Figure 2). Regarding cartilage fate, in regions where the octahedral shear strain exceeded a threshold value ($\varepsilon^{fibrocartilage}$), fibrocartilage formed. Both CCs and FCs became hypertrophic when the oxygen tension exceeded a specific value

($O_2^{hypertrophic}$), however this process was inhibited by sufficiently large magnitudes of strain ($\varepsilon^{hypertrophy} < \varepsilon^{oct,\ shear} < \varepsilon^{fibrocartilage}$).

The model was updated to include a condition whereby a higher oxygen tension was required to induce hypertrophy in stable cartilage. Motivated by the findings of Liu *et al.* (12) and Leijten *et al.* (15), a region of phenotypically stable cartilage was considered to have formed after cartilage was predicted within a specific region for a sufficiently long period of time (T^{stable}); following this a higher oxygen tension ($O_2^{hyp,\ stable}$) was required to induce hypertrophy. In addition to this, it was also assumed that stable cartilage was unable to transdifferentiate into fibrocartilage.

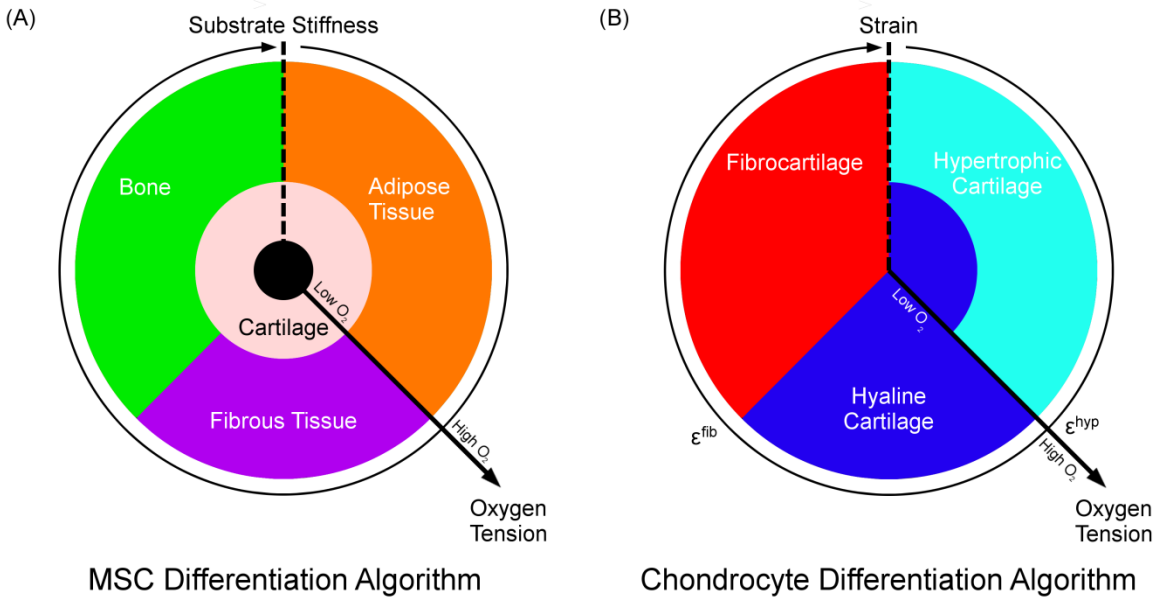

Figure 2: Tissue differentiation algorithm where (A) MSC fate is governed by a combination of the substrate stiffness and local oxygen tension and (B) chondrocyte fate is governed by the octahedral shear strain and the local oxygen tension.

2.8 Bilayer and Trilayer Models

Based on the scaffold design described by Da *et al.* (22), in both the bilayer and trilayer scaffold simulations, a total of 2 x 10^5 of the lattice points in the chondral phase were initialised as CCs and 5 x 10^5 lattice points in the osseous phase were initialised as OBs. It was assumed that there was a homogeneous distribution of cells throughout the construct. Furthermore, in the simulations, MSCs from the native tissue were able to migrate into the scaffold at day 0. This was implemented by assigning 5 % of the lattice points on the cancellous bone surface to MSCs. In the trilayer layer model, cells and blood vessels were unable to pass through the compact layer until it had been completely absorbed. This absorption process was considered to have finished at the time $T = T^{degrade}$, at which point the compact layer was

no longer present in the model. In each simulation the compact layer was absorbed over a period of 4 weeks ($\Delta T^{degrade}$ = 4 weeks), as a result the absorption process was initiated at the time point ($T = T^{degrade} - \Delta T^{degrade}$). In addition to this, it was assumed that the compact layer inhibited the diffusion of oxygen between the osseous and chondral phases. To model this, a lower diffusion coefficient ($G^{compact} = G_0/5$) was initially applied to this region. In order to characterise the absorption of this layer, the diffusion coefficient was updated using a linear model where $G = G^{compact}$ at $T \leq T^{degrade} - \Delta T^{degrade}$ up to $G = G_0$ at $T \geq T^{degrade}$.

2.9 Study Design

In the first part of this study, the updated model was used to simulate the time-course of tissue differentiation observed during the spontaneous repair process within an osteochondral defect (i.e. an empty defect). In this case, motivated by the *in vivo* study conducted by Liu et al. (12), the parameter T^{stable} was varied between 2 weeks and 12 weeks. The results of these simulations were compared to the results obtained using a model where blood vessel growth was independent of the tissue phenotype ($T^{stable} = \infty$).

In the second part of this study the updated model was used to predict the course of healing in an osteochondral defect treated with the different types of scaffolds developed by Da *et al.* (22). Firstly the model predicted the course of healing in a defect treated with the bilayer (compact layer free) scaffold (Figure 1B). In these simulations the parameter T^{stable} was varied between 8, 10 and 12 weeks in order to examine the effect that the maturation time of cartilage has on the predicted pattern of healing. Following this the model was used to predict the course of healing observed in a defect treated with the trilayer (compact layer) scaffold (Figure 1C). The purpose of this part of the study was to examine the effect that the absorption time of the compact layer has on the predicted course of healing. In this simulation, T^{stable} = 10 weeks and the parameter $T^{degrade}$ was varied between 4, 6, 8, 10 and 12 weeks. This was based on the findings of Da *et al.* (22) who reported that the scaffold materials had been completely absorbed after three months *in vivo*.

In the final part of this study, models were developed which simulated the course of healing in an osteochondral defect following treatment with either a cell-free bilayer scaffold or a cell-free trilayer scaffold. It was assumed that in these models the healing response was initiated by MSCs which migrated into the scaffold from the exposed cancellous bone at day 0. In both models the parameter T^{stable} = 10 weeks and in the trilayer simulation $T^{degrade}$ = 10

weeks. The purpose of this section was to examine the influence that the seeded cells have on tissue formation within the developed scaffold.

3 Results

3.1 Spontaneous repair within an empty osteochondral defect

The length of time required for MSC derived cartilage to become phenotypically stable (T^{stable}) was predicted to impact the patterns of tissue differentiation within the defect during the later stages of the repair process (Figure 3). In all of the models there was very little difference in the predicted behaviours for the first 8 weeks of the simulations. During this period, blood vessel growth was confined to the subchondral region of the defect (data not shown). For the opening 2 weeks of each simulation, bone formed in the base of the defect via intramembranous ossification. Cartilage tissue was predicted above this new bone, however, this soon underwent endochondral ossification as blood vessels grew further into defect. From week 4 onwards, bone formed mainly by further endochondral ossification. As the simulations progressed, the osseous front advanced towards the chondral phase of the defect until by week 8 it had reached the native subchondral bone.

By week 12, the spatial patterns of tissue differentiation predicted by the various models had begun to differ. In the original model ($T^{stable} = \infty$), the subchondral plate continued to advance until by week 24 the majority of the defect was composed of bone. In the updated models, the general trend was that T^{stable} governed the quantity of stable cartilage which was present in the chondral phase at weeks 12 and 24 (Figure 4). When this value was low stable cartilage formed at an earlier time point. This in turn meant that the advancing vascular network and subchondral plate were halted closer to the base of the defect. As T^{stable} increased, the quantity of bone predicted in the chondral phase at weeks 12 and 24 increased as the volume of cartilage decreased. Finally, in the simulations where $T^{stable} \geq 10$ the pattern of healing was the same as the pattern predicted by the model where $T^{stable} = \infty$.

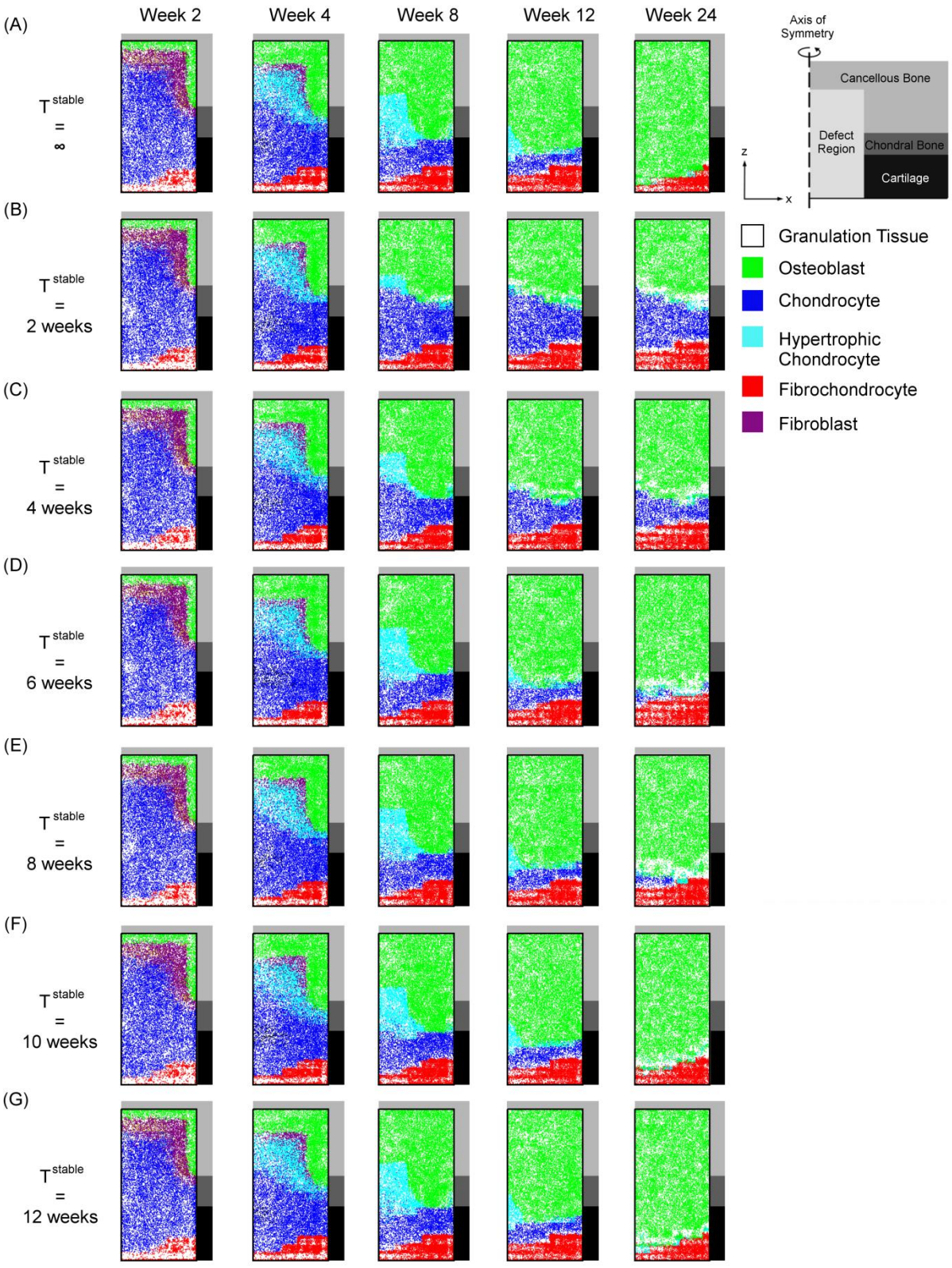

Figure 3: Model predictions of cell differentiation at different times during the spontaneous repair of an osteochondral defect using: (A) our previous tissue differentiation algorithm where angiogenesis was independent of the tissue phenotype and (B - G) the updated model where the parameter T^{stable} was varied between (B) 2 weeks (C) 4 weeks (D) 6 weeks (E) 8 weeks (F) 10 weeks and (G) 12 weeks.

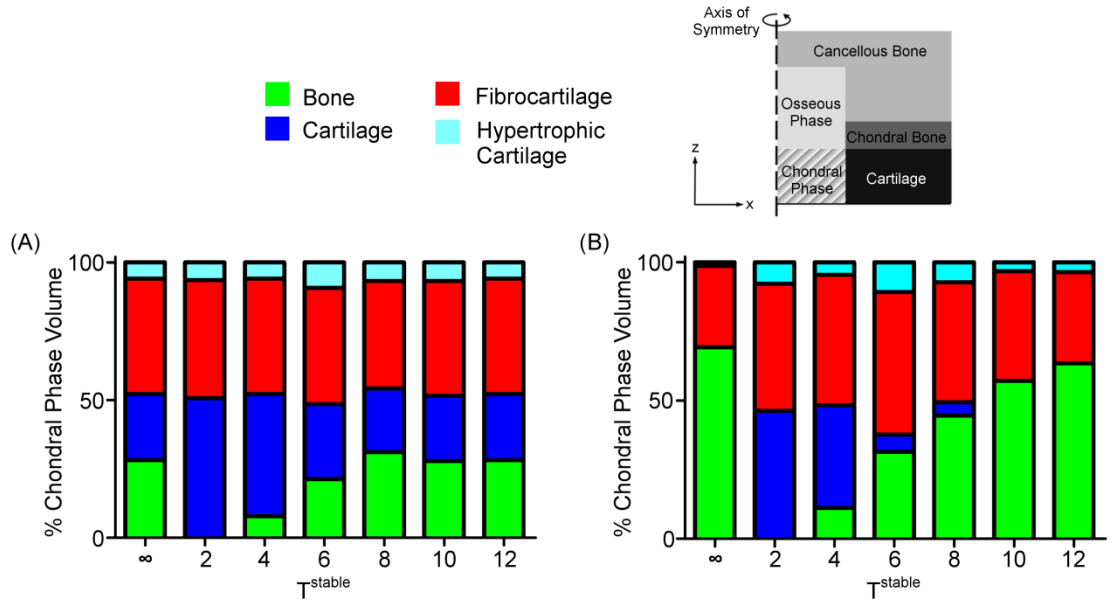

Figure 4: The relative volume of the different tissue phenotypes predicted within the chondral phase of the osteochondral defect at the (A) 12 week and (B) 24 week time points for different values of T^{stable}.

3.2 Osteochondral defect treated with a bilayer scaffold

The updated tissue differentiation algorithm was then used to predict the pattern of healing within an osteochondral defect treated with the bilayered scaffold (Figure 5). For the first 6 weeks of the simulations this parameter had no effect on the predicted pattern of healing. Over this period, cartilage and a small region of fibrocartilage formed in the chondral layer of the defect while bone formed in the osseous phase. This mineralised tissue formed through a mixture of intramembranous and endochondral ossification. Regarding the latter process, regions of cartilage initially formed in the osseous phase as the invading MSCs differentiated into CCs. This occurred as a result of the low oxygen environment present in the core of the bilayer scaffold at the early stages of the simulations. This was eventually converted to bone however as blood vessels grew further into the osseous phase as the simulation continued.

From week 12 onwards, the parameter T^{stable} had an effect on the predicted pattern of healing. Similar to the models of the spontaneous repair process, this parameter affected the quantity of stable cartilage which was predicted in the chondral phase of the defect by weeks 12 and 24 (Figure 5B & C). In the simulation where T^{stable} = 8 weeks the subchondral plate had become plane with the native bone by week 12. By the end of the simulation, only a small portion of this tissue had advanced into the chondral phase, the majority of which was stable cartilage. Conversely, in the simulations where either T^{stable} = 10 weeks or T^{stable} = 12 weeks,

mineralised tissue had begun to form in the chondral phase of the defect by week 12. At this point the advance of the bone front had stopped and there was very little difference in the spatial pattern of bone predicted at 12 weeks and the pattern predicted at 24 weeks. Over this period the presence of the subchondral plate in the chondral phase increased the magnitude of the local strains at the surface of the defect, this in turn resulted in an increase in the quantity of fibrocartilage present in the subchondral phase.

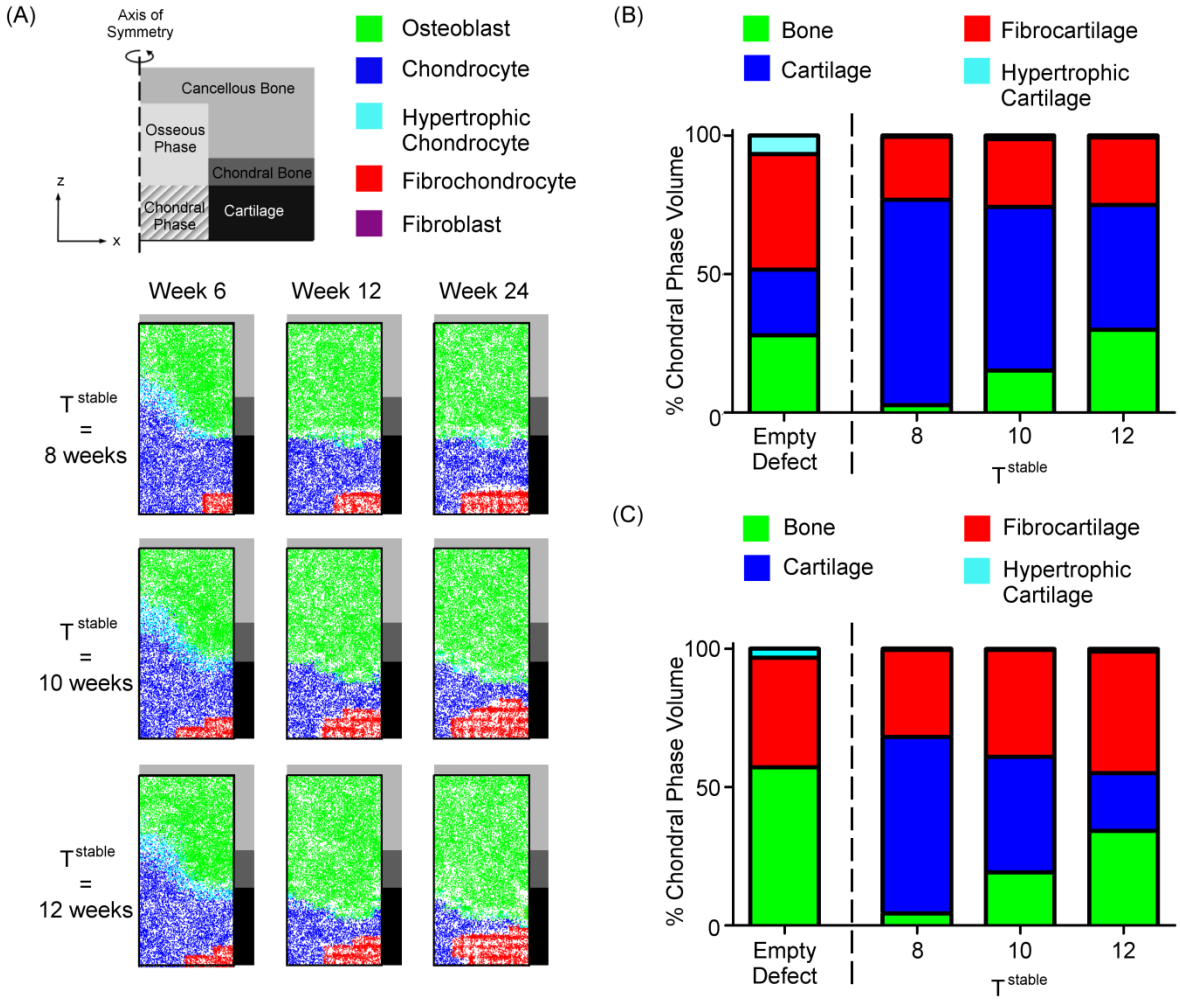

Figure 5: Results of the simulations of an osteochondral defect treated with the bilayer scaffold developed by Da et al. (22). *(A) Model predictions of cell differentiation for different values of the parameter T^{stable}. (B; C)The relative volume of the different tissue phenotypes predicted within the chondral phase of an empty defect (T^{stable} = 10 weeks) and a defect treated with the bilayer scaffold at the (B) 12 week and (C) 24 week time points for different values of T^{stable}.*

3.3 Osteochondral defect treated with a trilayer scaffold

The developed models of an osteochondral defect treated with the trilayer scaffold all followed the same general pattern of repair (Figure 6). In the same way as predicted in the bilayer scaffold simulations, bone formed in the osseous region through a combination of intramembranous and endochondral ossification. At the same time, cartilage formed in the chondral layer of the scaffold. As the models progressed, unlike in the empty defect or the

bilayer scaffold simulations, blood vessel growth was restricted to the osseous phase by the compact layer (Figure 7). In all simulations, by week 12 this layer had been absorbed and the osseous phase was composed entirely of bone while the chondral phase was composed mainly of cartilage with a small region of fibrocartilage present at the surface of the defect. At this time point the parameter $T^{degrade}$ had a small effect on the volume of bone predicted in the chondral phase (Figure 6B).

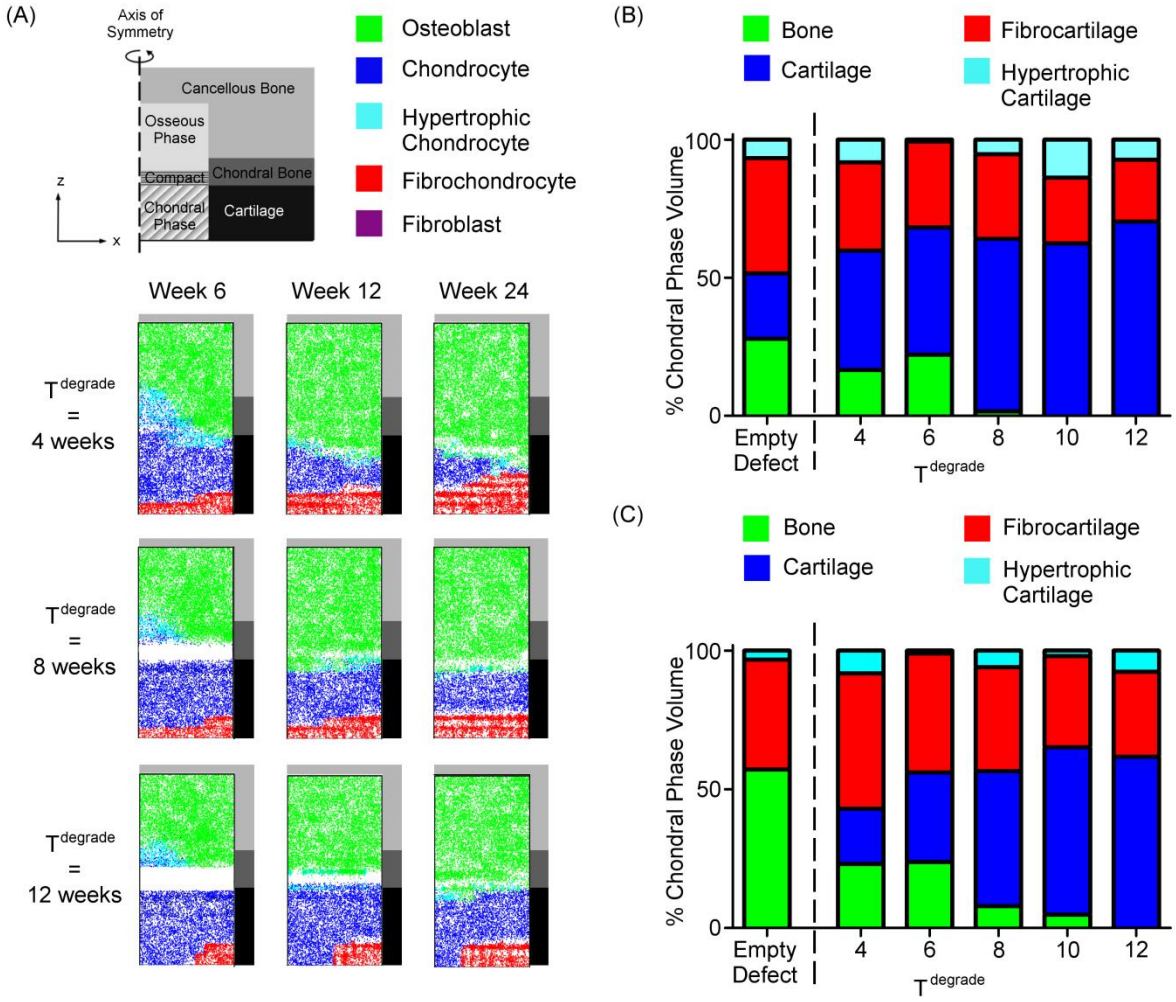

Figure 6: Results of the simulations of an osteochondral defect treated with the trilayer scaffold developed by Da et al. (22). *(A) Model predictions of cell differentiation for different values of the parameter $T^{degrade}$. (B; C)The relative volume of the different tissue phenotypes predicted within the chondral phase of an empty defect (T^{stable} = 10 weeks) and a defect treated with the trilayer scaffold at the (B) 12 week and (C) 24 week time points for different values of $T^{degrade}$.*

By week 24, the influence that the parameter $T^{degrade}$ had on the volume of bone in the chondral phase became more apparent (Figure 6C). In general, the volume of bone was higher for smaller values of $T^{degrade}$. This resulted in there being a lower quantity of cartilage and, in the case where $T^{degrade}$ = 4 weeks, a higher quantity of fibrocartilage. In the simulations where $T^{degrade}$ < 8 weeks, the pattern of healing was similar to the pattern predicted in the bilayer

simulations. Conversely, in the simulations where $T^{degrade} \geq 8$ weeks, the models predicted that there was a higher quantity of cartilage and a lower quantity of fibrocartilage compared to the equivalent bilayer simulation. Finally, in the model where $T^{degrade} = 12$ weeks, no bone was predicted in the chondral phase of the defect.

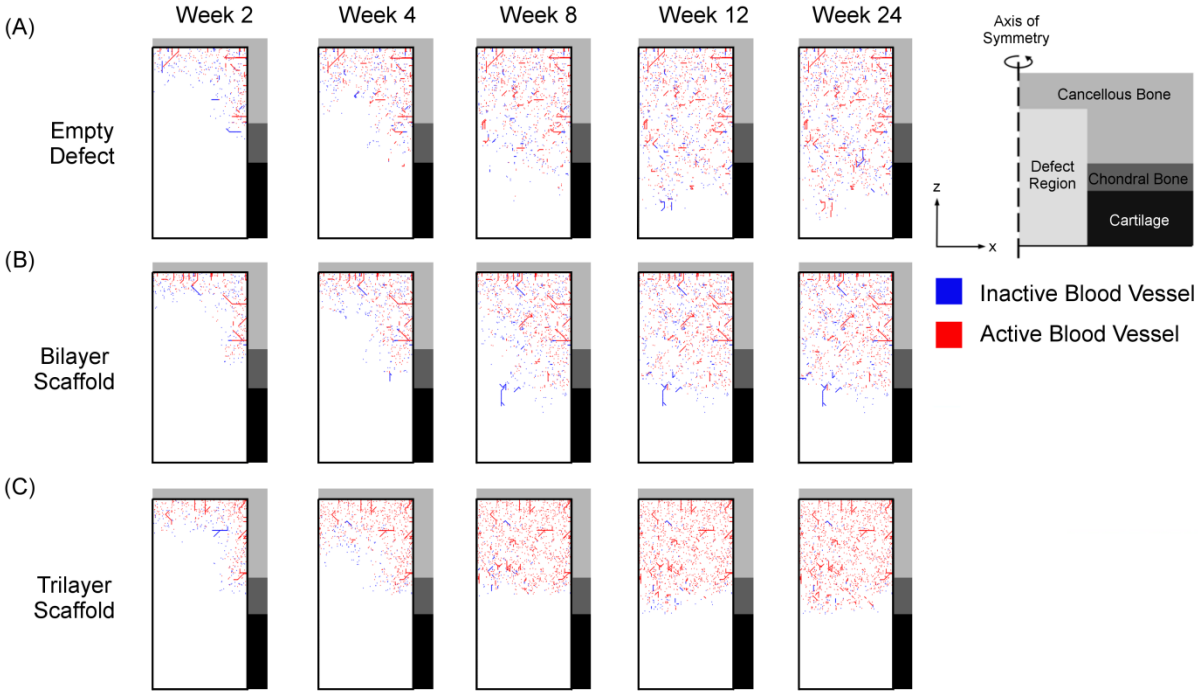

Figure 7: Comparison of the predicted spatial pattern of blood vessel formation at different time points between: (A) the model of the spontaneous repair process (B) the model of a defect treated with the bilayer scaffold and (C) the model of the defect treated with the trilayer scaffold. In all simulations $T^{stable} = 10$ weeks and for the trilayer simulation $T^{degrade} = 10$ weeks.

3.4 Osteochondral defects treated with cell-free scaffolds

In the simulation of an osteochondral defect treated with a cell free version of the bilayer scaffold the pattern of healing resembled the pattern predicted by the models of the spontaneous repair process (Figure 8). Bone initially formed in the base of the defect by means of intramembranous ossification while a region of cartilage formed above this in the core of the defect. Unlike in the models of the spontaneous repair process, the surface of the defect was relatively devoid of cells for the opening 4 weeks of the simulations, the result of this was that fibrocartilage was not observed in this region until week 8. By this stage, the bone front had begun to advance towards the surface of the defect as the cartilage in the core was ossified via endochondral ossification. Similar to the spontaneous repair process, stable cartilage did not have sufficient time to form before it was vascularised. The result this was that the subchondral plate continued to advance until by week 24 the majority of the

chondral region was composed of bone. By this stage, the only other tissue which remained in the defect was fibrocartilage.

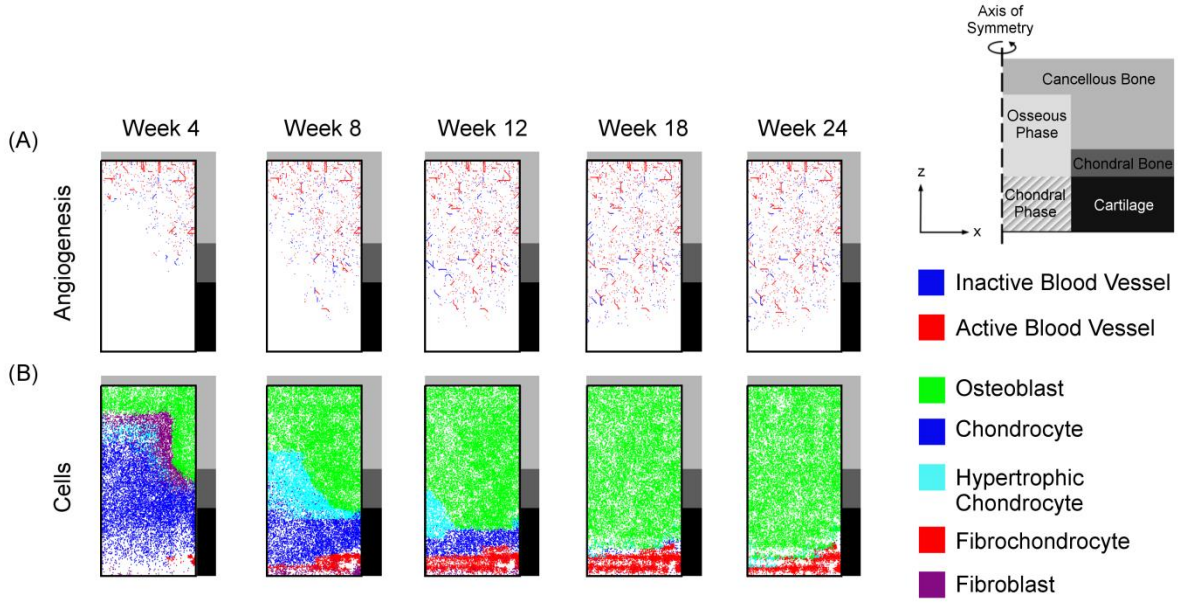

Figure 8: Model predictions of the spatial and temporal pattern of (A) angiogenesis and (B) cell differentiation in the simulation of an osteochondral defect treated with a cell-free bilayer scaffold developed by Da et al.(22) .

Stable cartilage also failed to form in the model of an osteochondral defect treated with a cell-free trilayer scaffold (Figure 9). For the opening 10 weeks of this simulation, the compact layer confined blood vessel growth, as well as cell proliferation and migration to within the osseous phase of the defect. The result of this was that, until this layer was absorbed, the pattern of healing resembled that of a chondral defect i.e. no healing response was predicted within the chondral phase. Following the absorption of the scaffold blood vessels began to form within the chondral phase, this in turn allowed cells to proliferate and form new tissue within this region. For the first few weeks, this new tissue was composed of a mixture of fibrocartilage and fibrous tissue. As the simulation progressed, the fibrous tissue was replaced with bone which in turn caused the upwards migration of the bone plate. Finally by week 24, similar to the model of the defect treated with a bilayer scaffold, the chondral region was composed of a mixture of bone and fibrocartilage.

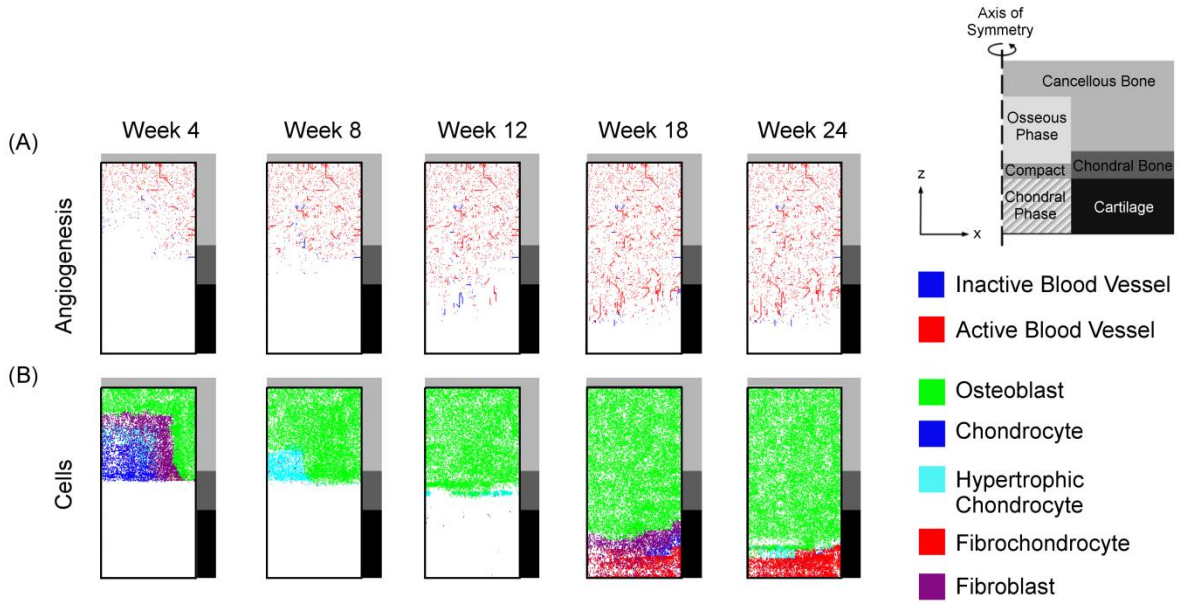

Figure 9: Model predictions of the spatial and temporal pattern of (A) angiogenesis and (B) cell differentiation in the simulation of an osteochondral defect treated with a cell-free trilayer scaffold developed by Da et al.(22)

4 Discussion

The objective of this study was to develop a computational model to better understand the potential mechanisms which may be utilised by TE strategies to regenerate the damaged tissues within an osteochondral defect. The overall goal was to develop a computational model of the experimental study conducted by Da *et al.* (22) in which the authors reported successful healing of an osteochondral defect following treatment with a novel multiphasic scaffold. As part of this, a previous *in silico* model of the spontaneous repair process within an osteochondral defect was updated to include a condition whereby mature cartilage was resistant to both terminal differentiation and vascularisation. This rule was developed based on studies which have shown that chondrocytes release anti-angiogenic factors such as chondromodulin-I (33,34) and troponin-I (35,36). Furthermore, studies have shown that, prior to subcutaneous implantation within a murine model, the time of in vitro culture of chondrogenically primed MSCs affects the cells' ability to resist terminal differentiation and vascularisation (12,15). The updated model was tested by using it to predict tissue formation during the spontaneous repair process within an osteochondral defect. Following this the model was used to simulate an osteochondral defect treated with different variations of the multiphasic scaffold developed by Da *et al.* (22). By comparing the results of these different simulations we provided support for the study hypothesis that the success of the scaffold can be attributed to the compact layer which provided a functional barrier to angiogenesis until

stable cartilage had formed. These results suggest the importance of controlling angiogenesis when designing TE strategies for the treatment of osteochondral defects.

A previously developed model of the spontaneous repair process within an osteochondral defect was used to develop the rules whereby stable cartilage was resistant to hypertrophy and inhibited blood vessel formation. This model was able to predict the main stages of the repair process which had been experimentally observed in a number of different *in vivo* studies (45,46). For this reason the temporal and spatial pattern of healing predicted by the updated models were compared to the results of this simulation. The parameter T^{stable} was varied between 2 weeks and 12 weeks with the purpose of examining its influence on the spontaneous repair process. In the simulations where $T^{stable} < 10$ weeks an altered pattern of healing was observed whereby cartilage was predicted in the chondral phase of the defect by week 24. Conversely, in the simulations where $T^{stable} \geq 10$ weeks the updated model had very little effect on the predicted course of the spontaneous repair process. Interestingly, Liu *et al.* (12) reported that in order to induce MSCs to form stable cartilage, an *in vitro* culture time of greater than 8 weeks in chondrogenic media was required prior to subcutaneous implantation. For this reason, the models where $T^{stable} \geq 10$ weeks are considered most representative of the actual behaviour experimentally observed during the spontaneous repair process. These results provide support for the hypothesis that, during the spontaneous repair process, stable cartilage does not have sufficient time to form before it is vascularised and converted to bone via endochondral ossification.

Further support for the updated model was provided by the results of the simulations of an osteochondral defect treated with either the bilayer or trilayer scaffold developed by Da *et al.* (22). Both of these models were able to predict the features of healing which had been experimentally observed within this *in vivo* study. Regarding this, Da *et al.* (22) reported that, by 24 weeks, defects treated with either scaffold had formed cartilage and bone within the chondral and osseous phases respectively. This healing was more robust in the trilayer scaffold group where thicker cartilage was observed after 24 weeks, a feature which was also observed within the simulations. In addition to this, the authors also reported that the cartilage which formed in the trilayer scaffold group was histologically superior to the cartilage which formed in the bilayer scaffold group. This was also observed in the models in which there was a higher volume of cartilage predicted in the trilayer scaffold simulations ($T^{degrade} \geq 8$ weeks) compared to the bilayer scaffold simulations ($T^{stable} \geq 10$ weeks).

The developed models also provide support for the hypothesis that the success of the trilayer scaffold can be attributed to the compact layer which served to confine angiogenesis to the osseous region until stable cartilage had formed in the chondral phase. In the simulations where the parameter $T^{degrade} \leq 6$ weeks the predicted pattern of healing was similar to the pattern predicted in the bilayer scaffold models i.e. the compact layer had no effect on the pattern of healing. Conversely, in the simulations where $T^{degrade} > 6$ weeks a higher quantity of stable cartilage was predicted in the chondral phase of the defect by week 24. These findings suggest that the model hypothesis is correct on the condition that the compact layer remained within the defect for a minimum period of 8 weeks. Regarding this, although no study to our knowledge has examined the absorption rate of PLGA/TCP *in vivo*, it has been shown *in vitro* that when left in a buffer saline solution, PLGA/TCP did not start degrading until approximately 8 weeks (47,48). Following this, the tested material then degraded rapidly and, depending on the culture conditions (static vs. dynamic), took between 4 and 8 weeks to lose between 30 % and 70 % of its mass (47,48). While it has been shown that scaffold materials tend to have a higher absorption rate *in vivo* (49), these studies suggest that the compact layer is present within the defect for a sufficient amount of time to support the model hypothesis.

In the final part of this study, the benefit of the cell seeding and pre-culture steps were shown through the simulation of an osteochondral defect treated with cell free versions of either the bilayer or trilayer scaffolds. In both models the scaffold alone was not sufficient to promote regeneration of the damaged tissues. This is in agreement with TE studies which have examined the efficacy of cell free scaffolds as a means with which to treat osteochondral defects (50,51). In the case of the bilayer model, the predicted pattern of healing was similar to that observed in the model of the spontaneous repair process. The scaffold improved healing by a small degree as by both week 12 and week 24 there was a lower volume of fibrocartilage predicted in the chondral phase when compared to the quantity predicted in the equivalent model of spontaneous repair (i.e. $T^{stable} = 10$ weeks) (data not shown). This can be attributed to the increased stiffness of the scaffold compared to granulation tissue. In the case of the trilayer model, the scaffold had an adverse effect on healing when compared to spontaneous repair. The reason for this was that the compact layer served to inhibit the passage of cells from the exposed cancellous bone into the chondral phase. The result of this was that, although bone was able to form in the osseous phase of the defect, for the opening

12 weeks no tissue formed in the chondral phase. It is important to note that in the cell-free trilayer model, as the scaffold was absorbed, the elements in the chondral phase were replaced with granulation tissue. In reality however this could not happen because there were no cells present in this phase at the time of absorption. For this reason, the latter 12 weeks of the simulation are not considered representative of what would happen if a cell-free, trilayer scaffold was inserted into an osteochondral defect.

There are a number of limitations associated with this study which limit the predictive capacity of the developed models. The first of these was that a simplified mechanism was used to model the behaviour whereby stable cartilage inhibits vascularisation by releasing anti-angiogenic factors. While this behaviour is well established experimentally (33–36), in the current approach the release of these factors was not explicitly modelled. Instead it was assumed that angiogenesis was inhibited after blood vessels formed in an element which contained stable cartilage. The problem with this was that by not considering the diffusion of these factors, mature cartilage was unable to influence the surrounding tissues. This 'crosstalk' has been postulated to affect bone and cartilage formation (52) and is one of the mechanisms by which the compact layer in the trilayer scaffold was hypothesised to improve the regeneration of the damaged tissues (22). Another simplification was that stable cartilage had a binary effect on angiogenesis i.e. blood vessels either grew at a constant rate or were completely inhibited by stable cartilage. In reality, as a result of the growth factors released by the different cells phenotypes, the rate of blood vessels growth may vary both temporally and spatially within an osteochondral defect. In the case of this study, this may explain the reduced rate of bone formation experimentally observed at 12 weeks in defects treated with the bilayer scaffold compared to defects treated with the trilayer scaffold (22) (a feature not predicted within the developed *in silico* models). Regarding this mechanism, anti-angiogenic factors released by the chondrogenically primed MSCs in the chondral phase may have diffused into the osseous phase of the bilayer scaffold. This would have resulting in a reduced rate of angiogenesis and in turn, a slower rate of bone formation within this phase.

Despite these limitations the developed model was able to predict the main features of healing experimentally observed in osteochondral defects treated with the scaffolds designed by Da *et al.*(22). These simulations provided support for the hypothesis that the compact layer improved cartilage formation by confining angiogenesis to the osseous phase of the defect. This in turn provides support for the hypothesis which we suggested in a previous study; that

osteochondral defect repair could be enhanced by interventions where angiogenesis is promoted but confined to within the subchondral region of the defect (31). Regarding the design of such treatments, based on the findings of this study we suggest that, in order to promote the formation of stable cartilage, angiogenesis should be actively confined to the osseous phase for a period of 10 weeks. The length of this time period can be reduced however by pre-culturing MSCs under chondrogenic conditions prior to implantation within the defect.

5 References

1. Nukavarapu SP, Dorcemus DL. Osteochondral tissue engineering: current strategies and challenges. Biotechnol. Adv. [Internet]. Elsevier Inc.; **31**(5), 706, 2013 [cited 2014 Jul 15]; Available from: http://www.ncbi.nlm.nih.gov/pubmed/23174560
2. Vacanti JP, Langer R. Tissue engineering: the design and fabrication of living replacement devices for surgical reconstruction and transplantation. Lancet. **354 Suppl** , SI32, 1999;
3. Deng T, Jing L, Pang J, Liu B, Ke J. Construction of tissue-engineered osteochondral composites and repair of large joint defects in rabbit. J. Tissue Eng. Regen. Med. **8**(7), 546, 2012;
4. Jiang J, Tang A, Ateshian G a, Guo XE, Hung CT, Lu HH. Bioactive stratified polymer ceramic-hydrogel scaffold for integrative osteochondral repair. Ann. Biomed. Eng. [Internet]. **38**(6), 2183, 2010 [cited 2014 Sep 29]; Available from: http://www.ncbi.nlm.nih.gov/pubmed/20411332
5. Getgood AMJ, Kew SJ, Brooks R, Aberman H, Simon T, Lynn AK, et al. Evaluation of early-stage osteochondral defect repair using a biphasic scaffold based on a collagen-glycosaminoglycan biopolymer in a caprine model. Knee [Internet]. Elsevier B.V.; **19**(4), 422, 2012; Available from: http://dx.doi.org/10.1016/j.knee.2011.03.011
6. Sheehy EJ, Vinardell T, Buckley CT, Kelly DJ. Engineering osteochondral constructs through spatial regulation of endochondral ossification. Acta Biomater. [Internet]. Acta Materialia Inc.; **9**(3), 5484, 2013; Available from: http://dx.doi.org/10.1016/j.actbio.2012.11.008
7. Miot S, Brehm W, Dickinson S, Sims T, Wixmerten a., Longinotti C, et al. Influence of in vitro maturation of engineered cartilage on the outcome of osteochondral repair in a goat model. Eur. Cells Mater. **23**(August 2015), 222, 2012;
8. Re'Em T, Witte F, Willbold E, Ruvinov E, Cohen S. Simultaneous regeneration of articular cartilage and subchondral bone induced by spatially presented TGF-beta and BMP-4 in a bilayer affinity binding system. Acta Biomater. **8**(9), 3283, 2012;
9. Dormer NH, Singh M, Zhao L, Mohan N, Berkand CJ, Detamore M. Osteochondral interface regeneration of the rabbit knee with macroscopic gradients of bioactive signals. J. Biomed. Mater. Res. **100**(1), 162, 2012;
10. Dickhut A, Pelttari K, Janicki P, Wagner W, Eckstein V, Egermann M, et al. Calcification or dedifferentiation: Requirement to lock mesenchymal stem cells in a desired differentiation stage. J. Cell. Physiol. **219**(1), 219, 2009;
11. Qui YS, Shahgaldi BF, Revell WJ, Heatley FW. Observations of subchondral plate advancement during osteochondral repair: A histomorphometric and mechanical study in the rabbit femoral condyle. Osteoarthr. Cartil. **11**, 810, 2003;
12. Liu K, Zhou GD, Liu W, Zhang WJ, Cui L, Liu X, et al. The dependence of in vivo stable ectopic chondrogenesis by human mesenchymal stem cells on chondrogenic differentiation in vitro. Biomaterials. **29**(14), 2183, 2008;
13. Pelttari K, Winter A, Steck E, Goetzke K, Hennig T, Ochs BG, et al. Premature induction of hypertrophy during in vitro chondrogenesis of human mesenchymal stem cells correlates with calcification and vascular invasion after ectopic transplantation in SCID mice. Arthritis Rheum. **54**(10), 3254, 2006;
14. Vinardell T, Sheehy EJ, Buckley CT, Kelly DJ. A comparison of the functionality and in vivo phenotypic stability of cartilaginous tissues engineered from different stem cell sources. Tissue Eng. Part A. **18**(11-12), 1161, 2012;

15. Leijten J, Georgi N, Moreira Teixeira L, van Blitterswijk C a, Post JN, Karperien M. Metabolic programming of mesenchymal stromal cells by oxygen tension directs chondrogenic cell fate. Proc. Natl. Acad. Sci. U. S. A. [Internet]. 2014 [cited 2014 Sep 17]; Available from: http://www.ncbi.nlm.nih.gov/pubmed/25205812

16. Gerber HP, Ferrara N. Angiogenesis and bone growth. Trends Cardiovasc. Med. **10**(5), 223, 2000;

17. Gerber H-P, Vu TH, Ryan AM, Kowalski J, Werb Z, Ferrara N. VEGF couples hypertrophic cartilage remodeling , ossification and angiogenesis during endochondral bone formation. Nat. Med. **5**(6), 623, 1999;

18. Hunziker EB, Driesang IMK, Saager C. Structural barriar principal for growth factor based articular cartilage repair. Clin. Orthop. Relat. Res. **391**, S182, 2001;

19. Hunziker EB, Driesang IMK. Functional barrier principle for growth-factor-based articular cartilage repair. Osteoarthr. Cartil. **11**(5), 320, 2003;

20. Nagai T, Sato M, Kutsuna T, Kokubo M, Ebihara G, Ohta N, et al. Intravenous administration of anti-vascular endothelial growth factor humanized monoclonal antibody bevacizumab improves articular cartilage repair. Arthritis Res. Ther. **12**, R178, 2010;

21. Klinger P, Surmann-Schmitt C, Brem M, Swoboda B, Distler JH, Carl HD, et al. Chondromodulin 1 stabilizes the chondrocyte phenotype and inhibits endochondral ossification of porcine cartilage repair tissue. Arthritis Rheum. **63**(9), 2721, 2011;

22. Da H, Jia S-J, Meng G-L, Cheng J-H, Zhou W, Xiong Z, et al. The impact of compact layer in biphasic scaffold on osteochondral tissue engineering. PLoS One [Internet]. **8**(1), e54838, 2013 [cited 2014 Dec 7]; Available from: http://www.pubmedcentral.nih.gov/articlerender.fcgi?artid=3557302&tool=pmcentrez&rendertype=abstract

23. Wang C, Meng G, Zhang L, Xiong Z, Liu J. Physical properties and biocompatibility of a core-sheath structure composite scaffold for bone tissue engineering in vitro. J. Biomed. Biotechnol. **2012**, 2012;

24. Jia S, Liu L, Pan W, Meng G, Duan C, Zhang L, et al. Oriented cartilage extracellular matrix-derived scaffold for cartilage tissue engineering. J. Biosci. Bioeng. [Internet]. The Society for Biotechnology, Japan; **113**(5), 647, 2012; Available from: http://dx.doi.org/10.1016/j.jbiosc.2011.12.009

25. Burke DP, Kelly DJ. Substrate stiffness and oxygen as regulators of stem cell differentiation during skeletal tissue regeneration: a mechanobiological model. PLoS One [Internet]. **7**(7), e40737, 2012 [cited 2014 Apr 29]; Available from: http://www.pubmedcentral.nih.gov/articlerender.fcgi?artid=3404068&tool=pmcentrez&rendertype=abstract

26. Lacroix D, Prendergast PJ. A mechano-regulation model for tissue differentiation during fracture healing: analysis of gap size and loading. J. Biomech. [Internet]. **35**(9), 1163, 2002; Available from: http://www.ncbi.nlm.nih.gov/pubmed/12163306

27. Hori RY, Lewis JL. Mechanical properties of the fibrous tissue found at the bone-cement interface following total joint replacement. J. Biomed. Mater. Res. [Internet]. **16**(6), 911, 1982; Available from: http://www.ncbi.nlm.nih.gov/pubmed/7174716

28. Claes LE, Heigele C a, Neidlinger-Wilke C, Kaspar D, Seidl W, Margevicius KJ, et al. Effects of mechanical factors on the fracture healing process. Clin. Orthop. Relat. Res. [Internet]. (355 Suppl), S132, 1998; Available from: http://www.ncbi.nlm.nih.gov/pubmed/9917634

29. Yao J, Salo AD, Barbau-McInnis M, Lerner AL. Finite Element Modeling of Knee Joint Contact

Pressures and Comparison to Magnetic Resonance Imaging of the Loaded Knee. ASME Int. Mech. Eng. Congr. Expo. 2003.

30. Checa S, Prendergast PJ. A mechanobiological model for tissue differentiation that includes angiogenesis: a lattice-based modeling approach. Ann. Biomed. Eng. [Internet]. **37**(1), 129, 2009 [cited 2014 May 23]; Available from: http://www.ncbi.nlm.nih.gov/pubmed/19011968

31. O'Reilly A, Kelly DJ. The role of oxygen as a regulator of stem cell fate during the spontaneous repair of osteochondral defects. J. Orthop. Res.

32. Carlier A, Geris L, Gastel N Van, Carmeliet G, Oosterwyck H Van. Oxygen as a critical determinant of bone fracture healing — A multiscale model. J. Theor. Biol. [Internet]. Elsevier; **365**, 247, 2015; Available from: http://dx.doi.org/10.1016/j.jtbi.2014.10.012

33. Shukunami C, Hiraki Y. Role of cartilage derived anti-angiogenic factor, chondromodulin-1 during endochondral bone formation. Osteoarthr. Cartil. **9**(Supplement A), S91, 2001;

34. Hayami T, Funaki H, Yaoeda K, Mitui K, Yamagiwa H, Tokunaga K, et al. Expression of the cartilage derived anti-angiogenic factor chondromodulin-I decreases in the early stage of experimental osteoarthritis. J. Rheumatol. **30**(10), 2207, 2003;

35. Moses M a, Wiederschain D, Wu I, Fernandez C a, Ghazizadeh V, Lane WS, et al. Troponin I is present in human cartilage and inhibits angiogenesis. Proc. Natl. Acad. Sci. U. S. A. **96**(6), 2645, 1999;

36. Kern BE, Balcom IV JH, Antoniu B a., Warshaw AL, Fernández-del Castillo C. Troponin I peptide (Glu94-Leu123), a cartilage-derived angiogenesis inhibitor: In vitro and in vivo effects on human endothelial cells and on pancreatic cancer. J. Gastrointest. Surg. **7**(8), 961, 2003;

37. Pérez M a, Prendergast PJ. Random-walk models of cell dispersal included in mechanobiological simulations of tissue differentiation. J. Biomech. [Internet]. **40**(10), 2244, 2007 [cited 2014 May 23]; Available from: http://www.ncbi.nlm.nih.gov/pubmed/17173925

38. Hershey D, Karhan T. Diffusion Coefficients for Oxygen Transport in Whole Blood. AIChE. **14**(6), 969, 1968;

39. Epari DR, Lienau J, Schell H, Witt F, Duda GN. Pressure, oxygen tension and temperature in the periosteal callus during bone healing--an in vivo study in sheep. Bone [Internet]. **43**(4), 734, 2008 [cited 2014 Jul 25]; Available from: http://www.ncbi.nlm.nih.gov/pubmed/18634913

40. Holzwarth C, Vaegler M, Gieseke F, Pfister SM, Handgretinger R, Kerst G, et al. Low physiologic oxygen tensions reduce proliferation and differentiation of human multipotent mesenchymal stromal cells. BMC Cell Biol. [Internet]. **11**(11), 2010; Available from: http://www.biomedcentral.com/1471-2121/11/11

41. Isaksson H, van Donkelaar CC, Huiskes R, Ito K. A mechano-regulatory bone-healing model incorporating cell-phenotype specific activity. J. Theor. Biol. [Internet]. **252**(2), 230, 2008 [cited 2014 May 27]; Available from: http://www.ncbi.nlm.nih.gov/pubmed/18353374

42. Appeddu PA, Shur BD. Molecular analysis of cell surface fi-1 , 4-galactosyltransferase function during cell migration. Proc. Natl. Acad. Sci. U. S. A. **91**(March), 2095, 1994;

43. Malda J, Rouwkema J, Martens DE, Le Comte EP, Kooy FK, Tramper J, et al. Oxygen gradients in tissue-engineered PEGT/PBT cartilaginous constructs: measurement and modeling. Biotechnol. Bioeng. [Internet]. **86**(1), 9, 2004 [cited 2014 Aug 8]; Available from: http://www.ncbi.nlm.nih.gov/pubmed/15007836

44. Chae H-J, Kim S-C, Han K-S, Chae S-W, An N-H, Kim H-M, et al. Hypoxia induces apoptosie by caspase activation accompanying cytochrome c release from mitochondria in MC3T3E1 osteoclasts. P38 MAPK is is related in hypoxia-induced apoptosis. Immunopharmacol.

Immunotoxicol. [Internet]. **23**(2), 133, 2001; Available from: http://www.tandfonline.com/doi/full/10.1081/IPH-100103855

45. Shapiro F, Koide S, Glimcher MJ. Cell Origin and Differentiation in the Repair of Full-Thickness Defects of Articular Cartilage. J. Bone Jt. Surg. **75-A**(4), 532, 1993;

46. Orth P, Cucchiarini M, Kaul G, Ong MF, Gräber S, Kohn DM, et al. Temporal and spatial migration pattern of the subchondral bone plate in a rabbit osteochondral defect model. Osteoarthr. Cartil. **20**, 1161, 2012;

47. Wu L, Ding J. In vitro degradation of three-dimensional porous poly(D,L-lactide-co-glycolide) scaffolds for tissue engineering. Biomaterials. **25**(27), 5821, 2004;

48. Yang Y, Zhao Y, Tang G, Li H, Yuan X, Fan Y. In vitro degradation of porous poly(l-lactide-co-glycolide)/β-tricalcium phosphate (PLGA/β-TCP) scaffolds under dynamic and static conditions. Polym. Degrad. Stab. **93**(10), 1838, 2008;

49. Sung H-J, Meredith C, Johnson C, Galis ZS. The effect of scaffold degradation rate on three-dimensional cell growth and angiogenesis. Biomaterials. **25**(26), 5735, 2004;

50. Reyes R, Pec MK, Sánchez E, del Rosario C, Delgado a., Évora C. Comparative, osteochondral defect repair: Stem cells versus chondrocytes versus bone morphogenetic protein-2, solely or in combination. Eur. Cells Mater. **25**, 351, 2012;

51. Dahlin RL, Kinard L a., Lam J, Needham CJ, Lu S, Kasper FK, et al. Articular chondrocytes and mesenchymal stem cells seeded on biodegradable scaffolds for the repair of cartilage in a rat osteochondral defect model. Biomaterials [Internet]. Elsevier Ltd; **35**(26), 7460, 2014; Available from: http://dx.doi.org/10.1016/j.biomaterials.2014.05.055

52. Funck-Brentano T, Cohen-Solal M. Crosstalk between cartilage and bone: When bone cytokines matter. Cytokine Growth Factor Rev. [Internet]. Elsevier Ltd; **22**(2), 91, 2011; Available from: http://dx.doi.org/10.1016/j.cytogfr.2011.04.003

6 List of Tables

7 List of Figures

8 Supplementary Material

8.1 Iterative Model

Tissue differentiation within the osteochondral defect was simulated via an iterative procedure similar to the one outlined by Burke et al. (25) (**Error! Reference source not found.**). Briefly, a finite element model was used to predict the strain environment within the defect. The results of this were then used an inputs to a model of angiogenesis which was run in conjunction with models of cell migration, proliferation and death. Both the angiogenesis and cell models then provided inputs to an oxygen diffusion model which determined the oxygen environment within the defect. In this case the angiogenesis model was used to update the oxygen boundary condition while the cell model was used to update the oxygen consumption terms. Following this, cell differentiation was simulated based on the results of the oxygen and cell models. Using the tissue differentiation algorithm the phenotype of each element was calculated. Finally, the results of this were used to update the material parameters of each element of the FE model before the next iteration was run.

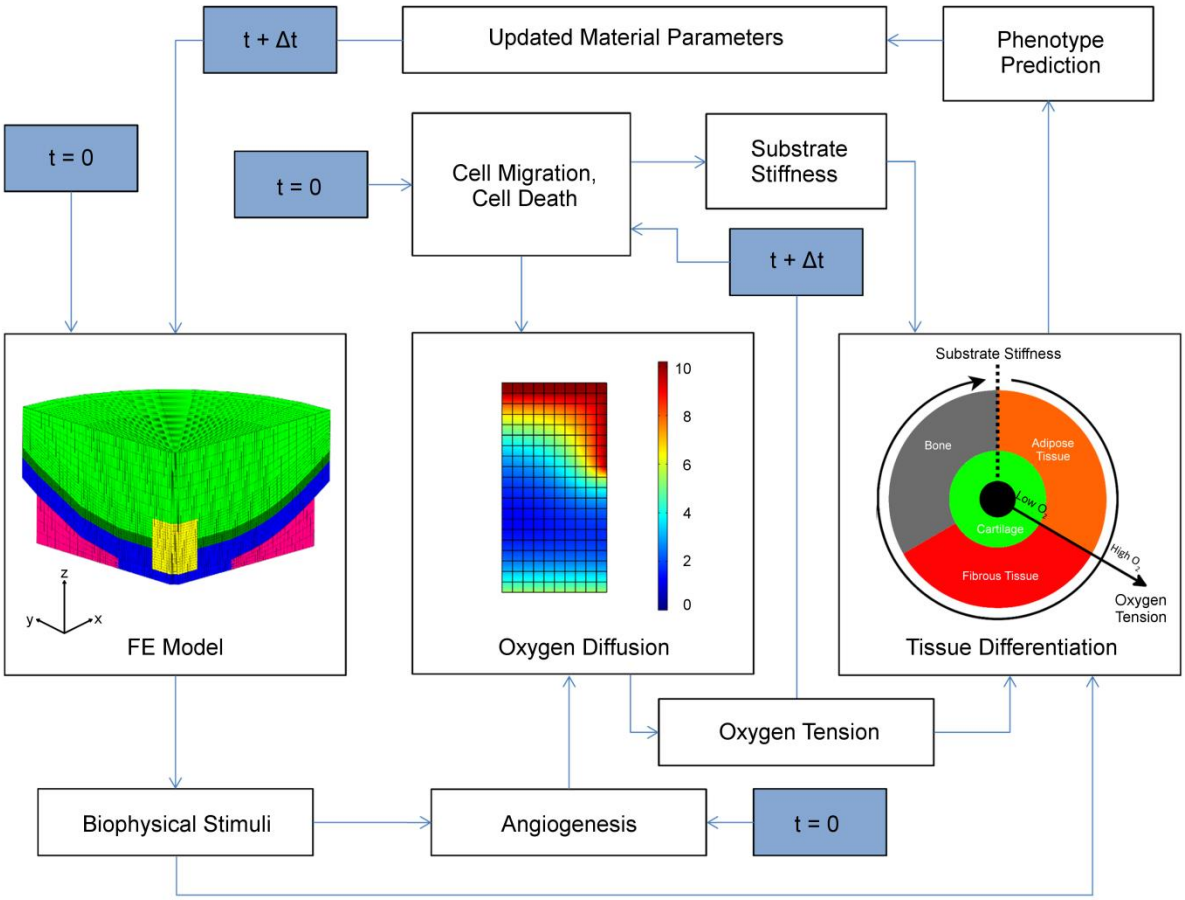

Supplementary Figure 1: Iterative procedure for the model of the spontaneous repair process within an osteochondral defect.

8.2 Oxygen Transport (Detailed)

Oxygen transport was modelled using the FE package COMSOL Multiphysics (version 4.3). The governing equation (Equation 1) was updated during each iteration based on the number of each cell type in a specific element.

$$\frac{dO_2}{dt} = G\nabla^2 O_2 - \sum_{n=1}^{6} \rho_n \frac{Q^{max,n} O_2}{K^{m,n} + O_2} + Q^{vessels}$$

Equation 1

Oxygen consumption was modelled separately for each cell phenotype using Michealas-Menten kinetics. The oxygen supply from the blood vessels within each element was modelled with $Q^{vessels}$ which was calculated using the relationship outlined in equation 2.

$$Q^{vessels} = \begin{cases} \dfrac{O_2^{vessels} - O_2}{K^{vessels}}, & O_2 < O_2^{vessels} \\ 0, & O_2 \geq O_2^{vessels} \end{cases}$$

In this case $K^{vessels}$ was a temporal smoothing term used to prevent irregular jumps in the oxygen concentration ($K^{vessels}$ = 10 s) while $O_2{}^{vessels}$ was the minimum oxygen concentration

within the element. $O_2^{vessels}$ was determined as a function of $v^{density}$ which in turn was the percentage of lattice points within the element which contained active ECs. A linear relationship was used to calculate $O_2^{vessels}$ where $O_2^{vessels}$ = 0 mol/mm^3 for $v^{density}$ = 0 up to a maximum of $O_2^{vessels}$ = 101.6 x 10^{-12} mol/mm^3 at $v^{density,\ max}$.

8.3 Tissue Differentiation Algorithm (Detailed)

In the developed models, MSCs differentiated into CCs in regions of hypoxia ($O_2 \leq O_2^{cartilage}$), while in normoxic regions ($O_2 > O_2^{cartilage}$) MSCs differentiated into OBs, FBs or adipocytes depending on the substrate stiffness. When the substrate stiffness was high, osteogenesis occurred while low substrate stiffness promoted adipogenesis (note: adipogenesis was excluded from the developed model). In addition to this, based on previous studies (25), FBs were replaced by OBs provided that they met the conditions for osteogenesis i.e. high substrate stiffness and normoxic oxygen tension. The substrate stiffness was determined based on the phenotype of the cells in the surrounding lattice points [3]. The stiffness was considered high if the differentiating MSC was within the vicinity of a mature OB. MSCs had a search radius of 2 lattice points in any direction when it came to determining the phenotype of the surrounding cells. It was also assumed that a newly formed OB had to have reached a certain age (Age^{cell} = 5 days) before it had synthesised sufficient matrix to affect the differentiation potential of the neighbouring cells.

Once an element had committed to a particular phenotype (either bone, cartilage, or fibrous tissue), any remaining MSCs in that element differentiated along that phenotypic pathway. An element was said to have committed to a particular phenotype if 50 % of the total allowable lattice points within the element contained cells (i.e. there had to be a minimum cell density of 0.5 x 10^5 cells/mm^3). Following this, the element was said to belong to the phenotype which made up the majority of cells.